

# Structures and Rotational Constants of Monocyclic Monoterpenes at DFT Cost by Pisa Composite Schemes and Vibrational Perturbation Theory

Published as part of *The Journal of Physical Chemistry A special issue "Francesc Illas and Gianfranco Pacchioni Festschrift"*.

Federico Lazzari, Lina Uribe, Silvia Di Grande, Luigi Crisci, Marco Mendolicchio, and Vincenzo Barone\*



Cite This: *J. Phys. Chem. A* 2025, 129, 503–517



Read Online

ACCESS |



Metrics & More

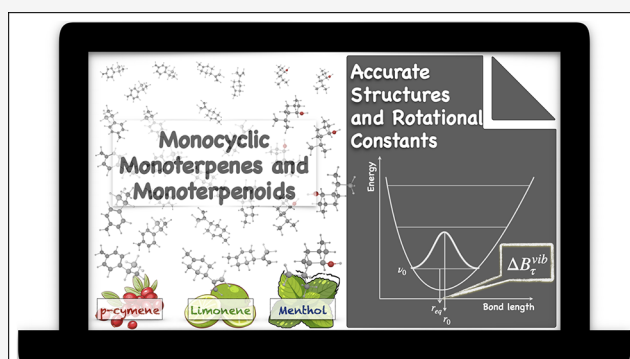


Article Recommendations



Supporting Information

**ABSTRACT:** The structures and rotational constants of prototypical monocyclic terpenes and terpenoids have been analyzed by a general computational strategy based on recent Pisa composite schemes (PCS) and vibrational perturbation theory at second order (VPT2). Concerning equilibrium geometries, a one-parameter empirical correction is added to bond lengths obtained by the revDSD-PBEP86 double hybrid functional in conjunction with a slightly modified cc-pVTZ-F12 basis set. The same functional and basis set give accurate harmonic frequencies, whereas the cheaper B3LYP hybrid functional in conjunction with a double- $\zeta$  basis set is employed to compute the semidiagonal cubic force constants needed to obtain vibrational corrections to the rotational constants in the framework of the VPT2 model. The final results obtained in this way show in most cases average deviations with respect to the experiment close to 0.1%, which correspond to errors around 1 mÅ and 0.1° for bond lengths and valence angles, respectively. The accuracy of the results has produced reliable estimates for species not analyzed yet experimentally. In addition to the intrinsic interest of the studied molecules, this article confirms that high-resolution spectroscopic studies of quite large systems can now be aided by a very accurate yet robust and user-friendly computational tool.

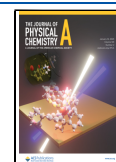


## 1. INTRODUCTION

The term “terpene” is often used ambiguously for any volatile, oily substance that is insoluble in water and typically has a resinous plant odor. More precisely, the term “terpene” should be reserved for hydrocarbons containing at least two isoprene units ( $\text{CH}_2=\text{C}(\text{CH}_3)\text{CH}=\text{CH}_2$ ), even though isoprene itself is not directly involved in the biosynthetic path of natural terpenes. Conversely, the name terpenoid should be used in the presence of additional functional groups, typically involving oxygen atoms.<sup>1,2</sup> Several terpenes and terpenoids are secondary metabolites of different organisms, including plants, animals, and fungi, and can be classified in terms of the number of isoprene units [ $(\text{C}_5)_n$ ] they contain. In this framework, monoterpenes/monoterpenoids contain two isoprene units ( $\text{C}_5$ )<sub>2</sub> and can be classified into acyclic, monocyclic, and bicyclic species.<sup>3</sup> The structures and spectroscopic parameters of several prototypical bicyclic monoterpenes and monoterpenoids have been recently investigated<sup>4</sup> by using several variants of the Pisa composite scheme (PCS).<sup>5</sup> In particular, reference energies and geometries of three prototypical compounds have been obtained by the very accurate PCS2 and PCS3 variants,<sup>6,7</sup> which are

rooted in explicitly correlated (F12) post-Hartree–Fock methods<sup>8,9</sup> and include both core–valence (CV) correlation and complete basis set (CBS) extrapolation. Then, the cheaper variant based on a double-hybrid density functional in conjunction with a triple- $\zeta$  basis set<sup>10</sup> was validated with reference to those values.<sup>4</sup> The equilibrium rotational constants were improved to spectroscopic accuracy (mean unsigned error (MUE) within 0.1%)<sup>11</sup> by means of a one-parameter bond-correction<sup>5,12,13</sup> and by taking into account vibrational corrections in the framework of vibrational perturbation theory at second order (VPT2)<sup>14–18</sup> based on a semidiagonal cubic force field computed by a cheaper hybrid functional in conjunction with a double- $\zeta$  basis set.

**Received:** October 22, 2024  
**Revised:** December 17, 2024  
**Accepted:** December 26, 2024  
**Published:** January 6, 2025



The main aim of this study is to apply the same computational approach to a representative panel of monocyclic monoterpenes and monoterpenoids, whose flexibility adds a further challenge to both the VPT2 model and the underlying electronic structure method.

Monocyclic monoterpenes and monoterpenoids can be classified into three families depending on the nature of their 1,4-disubstituted six-membered ring: benzene, cyclohexene, or cyclohexane.<sup>3</sup> We have selected *p*-cymene, anethole,<sup>19</sup> estragole,<sup>20</sup> thymol, and carvacrol<sup>21</sup> as examples of the first class; limonene, carvone, and perillaldehyde<sup>22</sup> as examples of the second class, and *p*-menthane, menthol, menthone, and isomenthone<sup>23</sup> as examples of the third class. Most of the selected compounds have been investigated experimentally, whereas for some of them, the computed results should provide reliable guesses for future investigations.

## 2. METHODS

A first sampling of potential energy surfaces (PES) ruled by soft degrees of freedom (exocyclic dihedral angles and ring puckerings) is carried out by the GFN2-XTB<sup>24</sup> semiempirical method in the framework of the metadynamics algorithm implemented in the CREST program.<sup>25</sup> Then, the different PCS variants employed to refine the results are labeled by a number giving the angular momentum of the largest (or unique) basis set used in the computation of valence electronic energies, preceded by a letter when explicitly correlated post-Hartree–Fock models are replaced by other quantum chemical methods. In particular, the *H* and *D* prefixes indicate the use of hybrid and double hybrid functionals, respectively. A further *B* letter specifies the use of one-parameter bond corrections in place of explicit computations of CV correlation and CBS extrapolation. In particular, the energy minima found in the preliminary exploration and lying below a predefined threshold are refined at the B3LYP level<sup>26–28</sup> in conjunction with the 6–31+G\* basis set<sup>29–31</sup> and augmented by the empirical D3BJ dispersion.<sup>32,33</sup> This combination of density functional and basis set will be referred to in the following as HPCS2. Then, the structures lying within a narrower threshold above the absolute energy minimum are refined with the revDSD-PBEP86 double hybrid functional, again augmented by the empirical D3BJ dispersion<sup>32–34</sup> in conjunction with the 3F12<sup>–</sup> basis set,<sup>5</sup> which is obtained from its standard cc-pVTZ-F12 (3F12) counterpart<sup>35</sup> by removing *d* functions on first-row atoms and replacing the two *f* functions on second- and third-row atoms by a single *f* function taken from the cc-pVTZ basis set.<sup>36</sup> This combination of the density functional and basis set will be referred to in the following as DPCS3.

The different energy thresholds depend on the system and the spectroscopic technique of interest. In general terms, a conservative limit for the relative stability of detectable species is around 900 cm<sup>–1</sup> (which corresponds to a relative population of around 1% at room temperature, where  $kT/hc = 207$  cm<sup>–1</sup>).<sup>5,37,38</sup> As a consequence, the thresholds employed in the present work for the acceptance of semiempirical structures, HPCS2 geometry optimizations, and final DPCS3 refinement are 2500, 1500, and 1000 cm<sup>–1</sup>, respectively. Furthermore, relaxation to more stable structures can take place whenever the energy barriers ruling this process are sufficiently low, with a typical threshold around 400 cm<sup>–1</sup>.<sup>39–41</sup> With the aim of unraveling those fast relaxations, the most significant paths connecting adjacent minima are analyzed by means of HPCS2 relaxed scans along soft degrees of freedom, namely, exocyclic

dihedral angles and (for the species containing a cyclohexene or cyclohexane moiety) ring puckerings. These latter soft degrees of freedom can be described in terms of the so-called Cremer–Pople ring coordinates.<sup>42</sup> In particular, three coordinates of this kind are needed for six-membered rings: two puckering amplitudes ( $q_2$  and  $q_3$ ) and a phase angle ( $\phi_2$ ), which are related to the coordinates of the ring atoms ( $z_j$  with  $j = 1, \dots, 6$ ) perpendicular to the mean ring plane:

$$q_2 \cos(\phi_2) = \frac{1}{\sqrt{3}} \sum_{j=1}^6 z_j \cos\left[\frac{2\pi(j-1)}{6}\right] \quad (1)$$

$$q_2 \sin(\phi_2) = -\frac{1}{\sqrt{3}} \sum_{j=1}^6 z_j \sin\left[\frac{2\pi(j-1)}{6}\right] \quad (2)$$

$$q_3 = \frac{1}{\sqrt{6}} \sum_{j=1}^6 (-1)^{j-1} z_j \quad (3)$$

Note that  $q_2$  is positive-valued, whereas  $q_3$  can take either positive or negative values, and  $0 \leq \phi_2 < 2\pi$  (in radians). These coordinates can be replaced by an equivalent set ( $Q, \theta, \gamma$ ), where  $\gamma = \phi_2$ ,  $Q$  is the total puckering amplitude, and  $0 \leq \theta \leq \pi$  (in radians),

$$Q = \sqrt{q_2^2 + q_3^2} \quad (4)$$

$$\theta = \arctan\left(\frac{q_2}{q_3}\right) \quad (5)$$

allowing for the mapping of all types of puckering (at fixed  $Q$ ) on the surface of a sphere. Furthermore, the positions of the ring substituents can be defined in terms of the angle  $\alpha$  formed by the bond between the ring atom and the substituent with the normal to the average ring plane:<sup>43</sup>  $\alpha \approx 0$  or  $\alpha \approx \pi$  corresponds to axial (labeled by *ax*) substituents, while  $\alpha \approx \pi/2$  corresponds to an equatorial substituent (labeled by *eq*). The parameters  $q_2$ ,  $\phi_2$ ,  $q_3$ , and  $\alpha$  have been obtained using the code described in ref 44 and are available in GitHub (<https://github.com/lucianschan/RING>).

It is now widely recognized that the best realistic level of accuracy of computed rotational constants for molecules containing more than 2 or 3 atoms is of the order of 0.1%.<sup>5,11,45,46</sup> Since the rotational constants of all the studied molecules range from 400 to 4500 MHz, in the following, their values will be truncated to 0.1 MHz and semiexperimental (SE) equilibrium values ( $A^{\text{SE}}$ ,  $B^{\text{SE}}$ , and  $C^{\text{SE}}$ ) will be derived from their experimental ground state counterparts ( $A^0$ ,  $B^0$ , and  $C^0$ ) employing vibrational corrections ( $\Delta A^{\text{vib}}$ ,  $\Delta B^{\text{vib}}$ , and  $\Delta C^{\text{vib}}$ , collectively referred to as  $\Delta \text{Vib}$ ) computed from harmonic and semidiagonal cubic force fields in the framework of the VPT2 model.<sup>48,47</sup>

The magnitude of vibrational corrections is typically between 0.3% and 0.7% that of the corresponding equilibrium rotational constants. Since the relative errors of vibrational corrections computed at the HPCS2 level are usually of the order of 10%,<sup>48</sup> the ensuing error of the rotational constants is more than acceptable. At the same time, equilibrium geometries computed at the DPCS3 level are remarkably accurate but need further refinement to reach spectroscopic accuracy. Based on these premises, several PCS variants<sup>7,10,12,49</sup> have been developed to attain this accuracy for increasingly larger molecules.

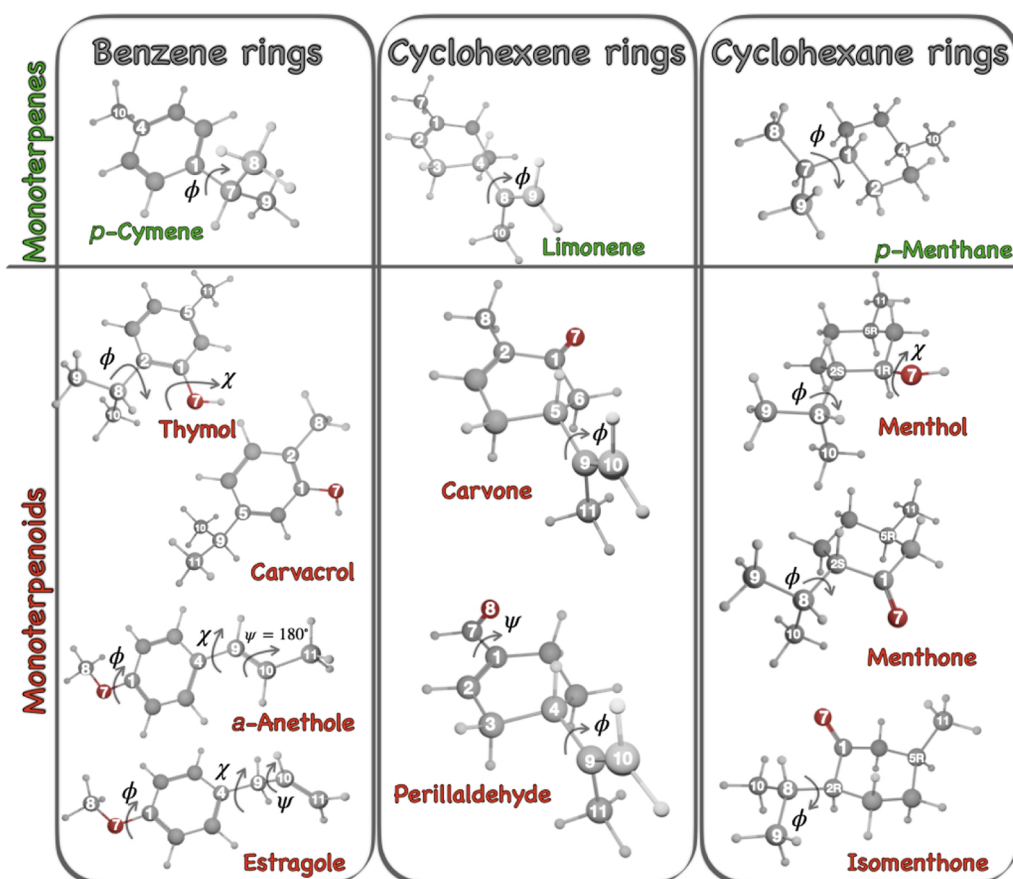


**Figure 1.** Structures, atom numberings (following the IUPAC rules), soft dihedral angles, and common names of the studied monocyclic monoterpenes and monoterpenoids containing a benzene, cyclohexene, or cyclohexane ring.

In the present study, equilibrium geometries have been obtained using the BDPCS3 variant, which improves DPCS3 geometries by incorporating one-parameter corrective terms (referred to as  $\Delta r^{\text{BCV}}$  for the CV contribution and  $\Delta r^{\text{BV}}$  for the valence contribution), which are applied exclusively to bond lengths:<sup>5</sup>

$$r_{ij}^{\text{BDPCS3}} = r_{ij}^{\text{DPCS3}} + \Delta r_{ij}^{\text{BCV}} + \Delta r_{ij}^{\text{BV}} \quad (6)$$

with

$$\Delta r_{ij}^{\text{BCV}} = -k\sqrt{n_i n_j - 1}(r_i^{\text{cov}} + r_j^{\text{cov}}) \quad (7)$$

and

$$\Delta r_{ij}^{\text{BV}} = \Delta r_{ij}^{\text{BCV}} \left[ \sqrt{|P_{ij} - 2|} - 1 \right] \left[ \delta(i, C)\delta(j, S) + \delta(i, S)\delta(j, C) + \sum_{X, Y \in \{C, N\}} \delta(i, X)\delta(j, Y) \right] \quad (8)$$

In the above equations, atomic numbers  $n_i$  and  $n_j$ , together with covalent radii  $r_i^{\text{cov}}$  and  $r_j^{\text{cov}}$  given in ref 50 rule the  $\Delta r^{\text{BCV}}$  contribution, while Pauling bond orders  $P_{ij}$ <sup>51</sup> and Kronecker  $\delta$ s are employed to tune the inclusion of the  $\Delta r^{\text{BV}}$  corrective terms for selected bonds only. The fitting of accurate bond lengths for a large panel of molecules containing H, C, N, O, F, P, S, and Cl

atoms led to  $k = 0.0011$ .<sup>5,12</sup> Note that eq 7 vanishes correctly for bonds between first-row atoms and that the final results can be obtained at the same cost as for the underlying geometry optimization at the DPCS3 level.

All the computations in the framework of density functional theory (DFT) have been performed with the Gaussian 16 package<sup>52</sup> and the BDPCS3 geometrical parameters have been obtained from a public domain website (<https://www.skies-village.it/proxima/pcsbonnds/>).<sup>13</sup>

### 3. RESULTS AND DISCUSSION

Figure 1 shows the three families of monocyclic monoterpenes and monoterpenoids (containing benzene, cyclohexene, and cyclohexane rings, respectively) investigated in the present work.

Among the species containing a benzene ring (first class), we have selected one monocyclic monoterpene (*p*-cymene), together with four monocyclic monoterpenoids (thymol, carvacrol, anethole, and estragole). All these molecules are natural compounds found in several plants (e.g., *Eucalyptus camaldulensis*, *Lippia sidoides*, *Pimpinella anisum*, and *Ocimum basilicum*) and have cardiovascular activities as vasorelaxants.<sup>2</sup>

The single soft degree of freedom (the  $\phi$  dihedral angle illustrated in Figure 1) of *p*-cymene gives rise to two equivalent low-energy minima. As a consequence, only one structure should be detectable in microwave (MW) spectra, but the very low dipole moment has hampered its unequivocal experimental characterization until now.

**Table 1.** Relative DPCS3 Electronic Energies ( $\Delta E$ ), HPCS2 Zero-Point Energies ( $\Delta ZPE$ ), Enthalpies [ $\Delta(\Delta H)$ ], and Entropies [ $\Delta(T\Delta S)$ ] at 298.15 K and 1 atm of the Studied Monocyclic Monoterpenes and Monoterpenoids containing a Benzene Ring<sup>a</sup>

	$\Delta E$	$\Delta ZPE^b$	$\Delta(\Delta H)^{cd}$	$\Delta(T\Delta S)^{ce}$	$\Delta E_a^f$
Thymol					
<i>g,a</i>	0.0	0.0	0.0	0.0	—
<i>g,s</i>	191.4	-225.9	46.1	51.5	—
<i>a,a</i>	192.4	-60.9	9.1	-28.9	—
<i>a,s</i>	608.5	-303.2	73.3	185.2	—
Carvacrol					
<i>a,a</i>	0.0	0.0	0.0	0.0	—
<i>s,a</i>	32.0	8.2	0.1	69.8	—
<i>a,s</i>	70.8	25.6	-18.0	-66.8	—
<i>s,s</i>	97.5	17.3	93.1	203.9	—
<i>a</i> -Anethole					
<i>s,a</i>	0.0	0.0	0.0	0.0	—
<i>s,s</i>	78.3	-44.6	37.1	326.5	—
Estragole					
<i>p,s</i>	0.0	0.0	0.0	0.0	<i>p,s</i> → <i>g,ac</i> : 890.7
<i>ac,ac</i>	17.5	-3.7	11.2	74.0	<i>ac,ac</i> → <i>g,ac</i> : 992.8
<i>g,ac</i>	54.3	1.7	4.1	36.7	<i>g,ac</i> → <i>ac,ac</i> : 697.8, 538.2 <sup>g</sup>

<sup>a</sup>The activation energies ( $\Delta E_a$ ) ruling the interconversion between low-energy structures of estragole are also given. All of the values are in  $\text{cm}^{-1}$ , and the ordering of the rotamers follows their  $\Delta E$ . <sup>b</sup>VPT2 anharmonic value. <sup>c</sup>Harmonic value. <sup>d</sup>Difference between the enthalpy at 298.15 K and at 0 K. <sup>e</sup>At 298.15 K. <sup>f</sup>Single point DPCS3 energies at HPCS2 geometries, including anharmonic  $ZPE_{\text{HPCS2}}$  corrections. <sup>g</sup> $\{g^-, ac^+\} \rightarrow \{ac^-, ac^-\}$ : 679.8;  $\{g^-, ac^+\} \rightarrow \{ac^+, ac^+\}$ : 538.2; see Figure 2.

Thymol and carvacrol are structural isomers, whose backbones are related to *p*-cymene, but also possess a hydroxyl group at the ortho or meta positions with respect to the isopropyl group. In the case of thymol, the rotation of the isopropyl group ( $\phi = \text{H}-\text{C}8-\text{C}2-\text{C}1$ ) leads to three different rotamers [*gauche*(+)( $g^+$ ), *gauche*(-)( $g^-$ ), and *antiperiplanar*(*a*), for dihedral angles of  $+40^\circ$ ,  $-40^\circ$ , and  $180^\circ$ ]. Since the  $g^+$  and  $g^-$  structures are equivalent, only two distinct structures (*g* and *a*) are generated. Then, the rotation of the OH group ( $\chi = \text{H}-\text{O}-\text{C}1-\text{C}2$ ) produces the *synperiplanar* (*s*, when the angle is close to  $0^\circ$ ) and *antiperiplanar* (*a*, when the angle is close to  $180^\circ$ ) rotamers. The four resulting structures will be referred to in the following as  $\{\phi, \chi\} = \{g, a\}$ ,  $\{a, a\}$ ,  $\{g, s\}$ ,  $\{a, s\}$  and correspond to the *trans A*, *trans B*, *cis A*, and *cis B* structures reported in ref 21. In contrast, the dihedral angle  $\phi = \text{H}-\text{C}9-\text{C}5-\text{C}2$  of carvacrol generates *s* ( $\phi = 0^\circ$ ) and *a* ( $\phi = 180^\circ$ ) conformers. The same energy minima are generated by rotation around the dihedral angle  $\chi = \text{H}-\text{O}-\text{C}1-\text{C}2$  in carvacrol and thymol. Therefore, the four rotamers of carvacrol are denoted  $\{\phi, \chi\} = \{a, a\}$ ,  $\{s, a\}$ ,  $\{a, s\}$ ,  $\{s, s\}$ , (*trans B*, *trans A*, *cis B*, *cis A*, respectively, following the nomenclature of ref 21).

Thymol and carvacrol have been investigated by Schmitz et al.<sup>21</sup> with a COMPACT spectrometer in the 2–8.5 GHz range. When the samples were heated to 373.15 K for thymol and 413.15 K for carvacrol three rotamers were detected in the first case and four rotamers in the second case. The barriers between the structures  $\{a, a\} \rightarrow \{s, a\}$  and  $\{a, s\} \rightarrow \{s, s\}$  are approximately  $1900 \text{ cm}^{-1}$ , whereas a barrier of about  $1300 \text{ cm}^{-1}$  rules the interconversion between the structures  $\{a, a\} \rightarrow \{a, s\}$ .<sup>21</sup> While the lack of efficient relaxation channels and the non-negligible populations of all low-energy minima (see Tables 1 and 2) would suggest that four structures should be observable in the MW spectra, only three species were reported in ref 21 for thymol. On the other hand, four carvacrol structures were detected, which are characterized by computed interconversion barriers exceeding  $800 \text{ cm}^{-1}$  (see Figure 2 in ref 21) and more

balanced populations for the different conformers (see Table 2). Since the intensities of rotational lines depend not only on the populations but also on the components of dipole moments, we computed both quantities for all of the studied molecules. However, comparable dipole moment components were always obtained for different low-energy minima of the same compound (see Table 2). As a consequence, we will make explicit references only to relative populations.

Anethole and estragole are also structural isomers, with a methoxy and propenyl group at the para position.

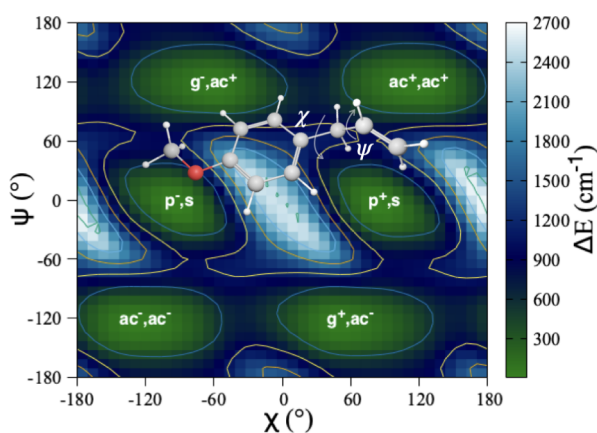
The anethole MW spectrum was recorded by Calabrese et al.<sup>19</sup> in the 59.6–74.4 GHz range. Although rotation along the  $\psi$  dihedral angle (see Figure 1) can generate *s* and *a* stereoisomers ( $\psi = 0^\circ/180^\circ$ , also referred to as *Z/E* or *cis/trans*), only the *a* stereoisomer was analyzed. Therefore, only two soft degrees of freedom (the dihedral angles  $\phi$  and  $\chi$ ) survive, and the  $C_s$  symmetry of *a*-anethole makes that only two distinct energy minima can be (and have actually been) detected in experimental spectra, labeled  $\{\phi, \chi\} = \{s, a\}$ ,  $\{s, s\}$ .

Estragole was analyzed using MW spectroscopy<sup>20</sup> in the millimeter range (48–72 GHz). The rotations around the dihedral angles  $\phi$ ,  $\chi$ , and  $\psi$  generate nine energy minima, with six of them being mirror images. Therefore, the following labeling (non requiring any specification of the  $\phi$  dihedral angle) is employed for the three energy minima giving distinct MW spectra:  $\{\chi, \psi\} = \{p, s\}$ ,  $\{ac, ac\}$ ,  $\{g, ac\}$ . The new labels *ac* and *p* are used for anticlinal ( $\phi$  or  $\chi = 120^\circ$ ) and *perpendicular* ( $\chi = \pm 90^\circ$ ) orientations. The results collected in Tables 1 and 2 suggest that three estragole structures should be present in the supersonic jet (since their computed populations are above 20%) unless effective interconversion channels are open. Figure 2 evidences a wider relaxation path for the  $\{g, ac\}$  conformer than for its counterpart  $\{p, s\}$  and the possibility of two different relaxation routes following either the  $\chi$  dihedral angle or a concerted change of  $\psi$  and  $\chi$  dihedral angles. The first path is governed by a lower energy barrier ( $538 \text{ cm}^{-1}$ ) only slightly higher than the usually accepted threshold of  $400 \text{ cm}^{-1}$ .<sup>4,53</sup>

**Table 2. Equilibrium Dipole Moments (in Debye) at the DPCS3 Level and Relative Populations (% $\chi_G$ ) at 298.15 K and 1 atm for all of the Studied Monocyclic Monoterpenes and Monoterpenoids**

	$ \mu_a $	$ \mu_b $	$ \mu_c $	$ \mu $	% $\chi_G^{a,b}$		$ \mu_a $	$ \mu_b $	$ \mu_c $	$ \mu $	% $\chi_G^{a,b}$
<i>p</i> -cymene						Perillaldehyde					
—	0.01	0.03	0.00	0.03	—	<sup>c</sup> <i>eq, ac</i> <sup>−</sup>	2.98	1.61	0.63	3.45	37.4
Thymol						<sup>c</sup> <i>eq, ac</i> <sup>+</sup>	3.10	1.79	0.43	3.60	11.4
<sup>c</sup> <i>g, a</i>	1.13	0.71	0.09	1.33	26.4 (24.0)	<sup>c</sup> <i>ax, s</i>	2.85	2.09	1.05	3.69	20.1
<sup>c</sup> <i>g, s</i>	1.25	0.77	0.02	1.46	51.5 (54.0)	<sup>c</sup> <i>eq, s</i>	2.96	1.46	0.32	3.32	30.6
<sup>c</sup> <i>a, a</i>	1.16	0.83	0.00	1.43	11.7 (10.1)	<i>ax, ac</i> <sup>−</sup>	3.05	2.15	1.05	3.88	0.4
<i>a, s</i>	1.10	1.05	0.04	1.52	10.4 (11.9)	<i>ax, ac</i> <sup>+</sup>	2.84	1.51	0.18	3.22	0.2
Carvacrol						<i>p</i> -menthane					
<sup>c</sup> <i>a, a</i>	1.07	0.59	0.00	1.22	27.6	<i>g</i> <sup>−</sup>	0.13	0.01	0.00	0.13	68.5
<sup>c</sup> <i>s, a</i>	0.90	0.89	0.00	1.27	31.8	<i>a</i>	0.04	0.08	0.01	0.09	31.5
<sup>c</sup> <i>a, s</i>	1.13	0.83	0.00	1.40	13.7	Menthol					
<sup>c</sup> <i>s, s</i>	0.92	0.99	0.00	1.35	27.0	<sup>c</sup> <i>g</i> <sup>+</sup> , <i>a</i>	1.32	0.08	0.80	1.54	46.7
<i>a</i> -Anethole						<i>g</i> <sup>+</sup> , <i>g</i> <sup>−</sup>	0.76	1.17	0.71	1.56	25.5
<sup>c</sup> <i>s, a</i>	1.06	0.30	0.00	1.10	22.6	<i>g</i> <sup>+</sup> , <i>g</i> <sup>+</sup>	0.84	1.18	0.88	1.69	17.0
<sup>c</sup> <i>s, s</i>	0.60	1.24	0.00	1.38	77.5	<i>a, a</i>	1.49	0.06	0.80	1.69	4.7
Estragole						<i>a, g</i> <sup>−</sup>	0.97	1.01	0.86	1.64	4.2
<sup>c</sup> <i>p, s</i>	0.48	1.10	0.34	1.25	31.6	<i>a, g</i> <sup>+</sup>	0.54	1.57	0.70	1.80	1.9
<sup>c</sup> <i>ac, ac</i>	0.82	1.13	0.13	1.40	40.1	Menthone					
<i>g, ac</i>	0.41	1.08	0.16	1.16	28.3	<sup>c</sup> <i>eq, eq, g</i> <sup>−</sup>	1.26	2.30	1.21	2.89	35.2
Limonene						<sup>c</sup> <i>eq, eq, g</i> <sup>+</sup>	1.24	2.56	0.49	2.88	39.4
<sup>c</sup> <i>eq, ac</i> <sup>−</sup>	0.40	0.35	0.35	0.63	45.8	<sup>c</sup> <i>eq, eq, a</i>	1.70	2.08	1.24	2.96	16.9
<sup>c</sup> <i>eq, ac</i> <sup>+</sup>	0.34	0.16	0.34	0.51	22.5	<i>ax</i> <sup>+</sup> , <i>ax</i> <sup>−</sup> , <i>g</i> <sup>−</sup>	0.06	2.78	1.59	3.20	8.5
<sup>c</sup> <i>eq, s</i>	0.30	0.66	0.17	0.74	24.3	Isomenthone					
<sup>c</sup> <i>ax, s</i>	0.11	0.60	0.28	0.67	4.9	<sup>c</sup> <i>ax</i> <sup>+</sup> , <i>eq, g</i> <sup>−</sup>	0.59	2.92	1.16	3.20	65.9
<i>ax, ac</i> <sup>−</sup>	0.59	0.10	0.03	0.60	1.5	<i>eq, ax</i> <sup>+</sup> , <i>g</i> <sup>−</sup>	0.98	2.29	1.45	2.88	12.9
<i>ax, ac</i> <sup>+</sup>	0.10	0.17	0.30	0.36	0.9	<i>eq, ax</i> <sup>+</sup> , <i>g</i> <sup>+</sup>	0.96	2.65	0.65	2.89	18.1
Carvone						<i>eq, ax</i> <sup>+</sup> , <i>a</i>	1.55	2.07	1.44	2.96	3.1
<sup>c</sup> <i>eq, ac</i> <sup>+</sup>	2.00	3.05	0.83	3.74	35.2						
<sup>c</sup> <i>eq, s</i>	2.18	3.25	0.68	3.97	29.5						
<sup>c</sup> <i>eq, ac</i> <sup>−</sup>	1.63	2.56	0.34	3.05	25.5						
<sup>c</sup> <i>ax, s</i>	2.48	3.16	0.74	4.08	3.8						
<sup>c</sup> <i>ax, ac</i> <sup>−</sup>	1.34	2.98	1.39	3.56	4.1						
<i>ax, ac</i> <sup>+</sup>	1.33	3.34	0.42	3.62	1.9						

<sup>a</sup>At 298.15 K. <sup>b</sup>The values in parentheses are at 375.15 K. <sup>c</sup>Experimentally observed structures.

**Figure 2.** Potential energy surface at the HPCS2 level for estragole.

However, this threshold depends on the temperature of the rare gas stream before expansion, and a threshold of 575  $\text{cm}^{-1}$  has been estimated for the temperature of 373 K at which the argon gas stream was heated in the experimental setup in which the estragole MW spectrum was recorded.<sup>20</sup> Therefore, the computed energy barrier is compatible with the relaxation of

the conformer  $\{g, ac\}$  to its more stable counterpart  $\{ac, ac\}$  and the consequent detection of only two structures ( $\{p, s\}$  and  $\{ac, ac\}$ ) in the recorded spectrum.

In Table 3, the equilibrium rotational constants of thymol, carvacrol, *a*-anethole, and estragole computed by different methods are compared with their SE counterparts, which have been obtained by combining the HPCS2 vibrational corrections (also reported) with the experimental ground state rotational constants. In Table 3 as well as in all of the other tables containing rotational constants, the results obtained by different computational approaches are accompanied by the corresponding absolute (MUE and MAX) and relative (MUE% and MAX%) mean and maximum unsigned errors.

The HPCS2 equilibrium rotational constants underestimate their SE counterparts by more than 1%, aligning more closely with the experimental ground-state values. As already pointed out in previous studies,<sup>4,54</sup> this trend results from a fortuitous compensation between the systematic overestimation of the equilibrium bond lengths at the HPCS2 level and the neglect of the bond length increase induced by vibrational averaging. The DPCS3 equilibrium rotational constants are significantly more accurate, with a relative mean unsigned error of 0.5%. However, the sought accuracy around 0.1% can be reached only after

**Table 3.** SE, HPCS2, DPCS3, and BDPCS3 Equilibrium Rotational Constants ( $A^{\text{eq}}$ ,  $B^{\text{eq}}$ , and  $C^{\text{eq}}$  in MHz), together with HPCS2 Vibrational Corrections ( $\Delta\text{Vib}$  in MHz) of Monocyclic Monoterpenes and Monoterpenoids Containing a Benzene Ring<sup>a</sup>

	Parameter	SE <sup>b</sup>	HPCS2	DPCS3	BDPCS3	$\Delta\text{Vib}$
<i>p</i> -cymene	$A^{\text{eq}}$	—	3255.0	3277.8	3288.8	29.5
	$B^{\text{eq}}$	—	724.6	731.5	733.8	5.1
	$C^{\text{eq}}$	—	683.1	689.0	691.1	4.4
Thymol <i>g, a</i>	$A^{\text{eq}}$	2051.2	2029.1	2045.0	2052.1	17.1
	$B^{\text{eq}}$	746.3	734.9	742.5	744.7	7.1
	$C^{\text{eq}}$	594.9	589.1	593.3	595.1	3.4
	MUE		13.1	3.9	0.9	
	MAX		22.0	6.2	1.6	
	MUE%		1.20	0.36	0.10	
	MAX%		1.53	0.51	0.21	
Thymol <i>a, a</i>	$A^{\text{eq}}$	2279.9	2228.9	2243.6	2250.7	18.9
	$B^{\text{eq}}$	714.3	706.0	711.5	713.8	5.4
	$C^{\text{eq}}$	616.1	609.6	613.9	615.8	4.3
	MUE		22.0	13.8	10.0	
	MAX		51.0	36.4	29.2	
	MUE%		1.49	0.78	0.47	
	MAX%		2.24	1.60	1.28	
Thymol <i>g, s</i>	$A^{\text{eq}}$	2068.2	2012.1	2034.5	2041.6	19.5
	$B^{\text{eq}}$	746.4	734.3	742.6	744.8	7.1
	$C^{\text{eq}}$	594.6	588.5	592.1	594.0	4.3
	MUE		24.8	13.3	9.6	
	MAX		56.1	33.7	26.6	
	MUE%		1.79	0.85	0.54	
	MAX%		2.71	1.63	1.29	
Carvacrol <i>a, a</i>	$A^{\text{eq}}$	2177.7	2154.3	2169.6	2177.1	18.6
	$B^{\text{eq}}$	675.9	667.1	673.4	675.5	5.1
	$C^{\text{eq}}$	581.7	574.8	579.6	581.4	4.1
	MUE		13.0	4.2	0.4	
	MAX		23.4	8.0	0.6	
	MUE%		1.30	0.39	0.06	
	MAX%		1.30	0.37	0.07	
Carvacrol <i>s, a</i>	$A^{\text{eq}}$	2304.4	2277.1	2295.3	2302.9	21.3
	$B^{\text{eq}}$	646.7	639.0	644.4	646.5	4.5
	$C^{\text{eq}}$	567.9	561.5	566.0	567.8	3.8
	MUE		13.9	4.4	0.6	
	MAX		27.4	9.1	1.5	
	MUE%		1.17	0.36	0.04	
	MAX%		1.20	0.40	0.07	
Carvacrol <i>a, s</i>	$A^{\text{eq}}$	2171.9	2145.7	2163.4	2170.9	19.0
	$B^{\text{eq}}$	677.3	668.8	674.9	676.9	5.0
	$C^{\text{eq}}$	582.3	575.4	580.3	582.1	4.1
	MUE		13.9	4.3	0.5	
	MAX		26.2	8.4	1.0	
	MUE%		1.22	0.36	0.05	
	MAX%		1.26	0.39	0.05	
Carvacrol <i>s, s</i>	$A^{\text{eq}}$	2296.0	2264.8	2286.6	2294.1	22.0
	$B^{\text{eq}}$	648.2	640.6	645.9	648.0	4.4
	$C^{\text{eq}}$	568.6	562.1	566.7	568.4	3.8
	MUE		15.1	4.6	0.8	
	MAX		31.3	9.5	1.9	
	MUE%		1.22	0.37	0.05	
	MAX%		1.36	0.41	0.08	
Anethole <i>s, a</i>	$A^{\text{eq}}$	4513.5	4492.3	4507.9	4521.9	35.4
	$B^{\text{eq}}$	460.9	454.4	458.6	460.0	3.3
	$C^{\text{eq}}$	420.4	414.8	418.5	419.7	2.7
	MUE		11.1	3.2	3.4	
	MAX		21.1	5.6	8.5	
	MUE%		1.07	0.36	0.19	
	MAX%		1.41	0.50	0.21	

Table 3. continued

	Parameter	SE <sup>b</sup>	HPCS2	DPCS3	BDPCS3	$\Delta$ Vib
Anethole <i>s, s</i>	A <sup>eq</sup>	3947.0	3936.2	3941.7	3955.2	31.4
	B <sup>eq</sup>	471.9	465.1	469.7	471.0	3.1
	C <sup>eq</sup>	423.7	418.2	421.9	423.1	2.4
	MUE		7.7	3.1	3.2	
	MAX		10.8	5.3	8.3	
	MUE%		1.01	0.34	0.18	
	MAX%		1.44	0.47	0.21	
Estragole <i>p, s</i>	A <sup>eq</sup>	2898.0	2871.5	2885.5	2894.9	20.4
	B <sup>eq</sup>	565.3	556.3	563.6	565.0	4.4
	C <sup>eq</sup>	545.2	537.2	543.9	545.3	3.8
	MUE		14.5	5.2	1.1	
	MAX		26.5	12.6	3.1	
	MUE%		1.32	0.32	0.05	
	MAX%		1.58	0.43	0.11	
Estragole <i>ac, ac</i>	A <sup>eq</sup>	3670.7	3640.0	3633.4	3647.1	27.5
	B <sup>eq</sup>	507.9	500.2	506.7	508.0	4.3
	C <sup>eq</sup>	462.9	456.7	462.5	463.7	3.3
	MUE		14.9	13.0	8.1	
	MAX		30.7	37.2	23.5	
	MUE%		1.23	0.45	0.27	
	MAX%		1.52	1.01	0.64	

<sup>a</sup>Absolute mean and maximum unsigned errors between computed and experimental rotational constants (MUE and MAX in MHz) and the corresponding relative values (MUE% and MAX%) are also reported. <sup>b</sup>SE equilibrium rotational constants obtained from the HPCS2 vibrational corrections computed in the present work and the experimental ground state rotational constants given in refs 19–21 for anethole, estragole, and thymol+carvacrol, respectively.

Table 4. Relative DPCS3 Electronic Energies ( $\Delta E$ ), HPCS2 Zero-Point Energies ( $\Delta ZPE$ ), Enthalpies [ $\Delta(\Delta H)$ ], and Entropies [ $\Delta(T\Delta S)$ ] at 298.15 K and 1 atm of the Studied Monocyclic Monoterpenes and Monoterpenoids Containing a Cyclohexene ring<sup>aa</sup>

	$\Delta E$	$\Delta ZPE^b$	$\Delta(\Delta H^c)^{cd}$	$\Delta(T\Delta S^e)^{ee}$	$Q^f$	$\theta^f$	$\gamma^f$	$\alpha^g$
Limonene								
<i>eq, ac</i> <sup>-</sup>	0.0	0.0	0.0	0.0	0.511	51.1	209.4	99.2
<i>eq, ac</i> <sup>+</sup>	65.3	27.8	-32.0	-86.2	0.506	51.2	208.5	99.0
<i>eq, s</i>	192.0	-2.1	-10.5	47.8	0.515	50.8	204.6	96.8
<i>ax, s</i>	203.0	67.6	-66.7	-260.2	0.506	50.5	33.6	171.6
<i>ax, ac</i> <sup>-</sup>	753.4	37.6	-0.9	84.0	0.471	50.2	30.4	171.0
<i>ax, ac</i> <sup>+</sup>	797.2	121.3	86.9	202.9	0.507	51.3	15.2	176.9
Carvone								
<i>eq, ac</i> <sup>+</sup>	0.0	0.0	0.0	0.0	0.487	53.6	72.7	98.9
<i>eq, s</i>	56.9	13.3	5.1	39.1	0.481	53.7	73.9	98.7
<i>eq, ac</i> <sup>-</sup>	111.8	-6.5	11.5	50.3	0.487	54.0	68.8	97.5
<i>ax, s</i>	273.7	89.1	-58.2	-158.5	0.491	53.7	247.7	177.7
<i>ax, ac</i> <sup>-</sup>	389.1	47.1	-49.6	-60.1	0.487	52.1	259.0	173.9
<i>ax, ac</i> <sup>+</sup>	496.1	55.6	-32.2	-88.0	0.412	51.2	259.6	169.5
Perillaldehyde								
<i>eq, ac</i> <sup>-</sup>	0.0	0.0	0.0	0.0	0.509	50.9	211.9	80.1
<i>eq, ac</i> <sup>+</sup>	93.6	36.8	-43.5	-159.5	0.506	51.1	213.2	80.5
<i>ax, s</i>	143.7	45.0	-30.7	28.9	0.508	50.1	34.6	8.1
<i>eq, s</i>	176.0	-4.7	1.4	131.1	0.513	50.6	206.7	82.7
<i>ax, ac</i> <sup>-</sup>	763.9	82.9	-36.1	-132.6	0.468	49.9	32.0	9.3
<i>ax, ac</i> <sup>+</sup>	852.0	135.0	-93.2	-196.4	0.497	50.7	17.6	4.1

<sup>a</sup>All the energetic values are in cm<sup>-1</sup>, except relative populations. All the geometric parameters are in degrees, except  $Q$ , which is in Å. The ordering of the rotamers follows their  $\Delta E$ . <sup>b</sup>VPT2 anharmonic value. <sup>c</sup>Harmonic value. <sup>d</sup>Difference between the enthalpy at 298.15 K and 0 K. <sup>e</sup>At 298.15 K. <sup>f</sup>See eqs 1–5 for definitions. The ring-puckering coordinates of the half-chair energy minimum of cyclohexene are  $Q = 0.490$  Å,  $\theta = 51^\circ$ , and  $\gamma = 30^\circ$ . <sup>g</sup>Referred to the isopropenyl group. See the main text for definition.

explicit consideration of CV correlation. Actually, the constant agreement within 0.1% between BDPCS3 and SE rotational constants for all the other terpenes (vide infra) suggests a

potential need for a reinvestigation of the MW spectrum of the {*a, a*} and {*g, s*} forms of thymol. In fact, 54 lines were fitted for {*g, a*} thymol, including transitions of *a*- and *b*-type, while only

**Table 5.** SE, HPCS2, DPCS3, and BDPCS3 Equilibrium Rotational Constants ( $A^{\text{eq}}$ ,  $B^{\text{eq}}$ , and  $C^{\text{eq}}$  in MHz), together with HPCS2 Vibrational Corrections ( $\Delta\text{Vib}$  in MHz) of the Studied Monocyclic Monoterpenes and Monoterpenoids Containing a Cyclohexene Ring<sup>a</sup>

	Parameter	SE <sup>b</sup>	HPCS2	DPCS3	BDPCS3	$\Delta\text{Vib}$
Limonene <i>eq</i> , $ac^-$	$A^{\text{eq}}$	3085.3	3053.6	3076.6	3086.3	27.3
	$B^{\text{eq}}$	723.2	713.5	720.7	723.2	6.1
	$C^{\text{eq}}$	684.7	675.3	682.1	684.5	5.5
	MUE		17.0	4.6	0.5	
	MAX		31.7	8.6	1.1	
	MUE%		1.25	0.33	0.03	
	MAX%		1.39	0.38	0.04	
Limonene <i>eq</i> , $ac^+$	$A^{\text{eq}}$	3081.5	3050.5	3073.2	3083.0	27.7
	$B^{\text{eq}}$	750.5	737.9	746.5	749.1	8.3
	$C^{\text{eq}}$	649.8	642.6	648.6	650.8	3.1
	MUE		16.9	4.4	1.3	
	MAX		31.0	8.2	1.5	
	MUE%		1.26	0.32	0.13	
	MAX%		1.68	0.53	0.19	
Limonene <i>eq</i> , $s$	$A^{\text{eq}}$	3067.4	3034.5	3057.5	3067.2	26.9
	$B^{\text{eq}}$	753.1	737.4	747.9	750.4	7.5
	$C^{\text{eq}}$	647.4	644.3	648.9	650.2	3.6
	MUE		17.2	5.3	1.9	
	MAX		32.9	9.9	2.8	
	MUE%		1.21	0.37	0.27	
	MAX%		2.08	0.70	0.43	
Limonene <i>ax</i> , $s$	$A^{\text{eq}}$	2183.9	2217.0	2170.8	2178.4	20.8
	$B^{\text{eq}}$	941.8	912.0	941.5	944.3	6.4
	$C^{\text{eq}}$	909.5	885.0	908.4	910.8	5.6
	MUE		29.1	4.8	3.2	
	MAX		33.1	13.1	5.5	
	MUE%		2.46	0.25	0.22	
	MAX%		3.16	0.60	0.27	
Carvone <i>eq</i> , $ac^+$	$A^{\text{eq}}$	2255.9	2231.9	2247.1	2254.8	18.7
	$B^{\text{eq}}$	661.1	652.6	658.9	661.2	4.8
	$C^{\text{eq}}$	583.8	576.1	581.7	583.7	4.1
	MUE		13.4	4.3	0.4	
	MAX		24.0	8.8	1.1	
	MUE%		1.22	0.36	0.03	
	MAX%		1.31	0.39	0.05	
Carvone <i>eq</i> , $s$	$A^{\text{eq}}$	2276.2	2252.8	2268.4	2276.1	19.2
	$B^{\text{eq}}$	679.3	669.5	676.4	678.8	6.4
	$C^{\text{eq}}$	557.5	550.2	555.7	557.6	3.0
	MUE		13.5	4.2	0.2	
	MAX		23.3	7.8	0.6	
	MUE%		1.26	0.37	0.03	
	MAX%		1.44	0.42	0.08	
Carvone <i>eq</i> , $ac^-$	$A^{\text{eq}}$	2230.9	2208.7	2224.2	2232.1	18.1
	$B^{\text{eq}}$	690.9	680.5	688.2	690.4	6.4
	$C^{\text{eq}}$	558.0	551.0	555.7	557.6	3.3
	MUE		13.2	3.9	0.7	
	MAX		22.2	6.7	1.2	
	MUE%		1.26	0.37	0.07	
	MAX%		1.52	0.41	0.08	
Carvone <i>ax</i> , $ac^-$	$A^{\text{eq}}$	1635.5	1628.2	1622.0	1628.1	13.7
	$B^{\text{eq}}$	910.8	889.6	912.8	915.4	5.9
	$C^{\text{eq}}$	785.2	768.0	784.9	787.0	4.7
	MUE		15.3	5.3	4.6	
	MAX		21.3	13.6	7.5	
	MUE%		1.66	0.36	0.40	
	MAX%		2.34	0.83	0.50	
Carvone <i>ax</i> , $s$	$A^{\text{eq}}$	1698.0	1692.8	1684.4	1690.6	10.2
	$B^{\text{eq}}$	887.5	866.9	888.3	890.9	9.3
	$C^{\text{eq}}$	777.9	760.4	777.8	779.9	6.6

Table 5. continued

	Parameter	SE <sup>b</sup>	HPCS2	DPCS3	BDPCS3	ΔVib
Perillaldehyde <i>eq</i> , <i>ac</i> <sup>-</sup>	MUE		14.5	4.9	4.2	
	MAX		20.6	13.6	7.4	
	MUE%		1.63	0.30	0.35	
	MAX%		2.32	0.80	0.44	
	A <sup>eq</sup>	2958.1	2931.5	2952.1	2961.5	25.4
	B <sup>eq</sup>	540.4	533.3	538.5	540.3	3.9
	C <sup>eq</sup>	513.9	506.8	511.8	513.5	3.7
	MUE		13.6	3.4	1.3	
Perillaldehyde <i>eq</i> , <i>ac</i> <sup>+</sup>	MAX		26.6	6.0	3.4	
	MUE%		1.20	0.33	0.07	
	MAX%		1.39	0.42	0.12	
	A <sup>eq</sup>	2981.7	2954.3	2975.3	2984.7	27.1
	B <sup>eq</sup>	552.1	543.2	549.3	551.2	5.1
	C <sup>eq</sup>	494.4	488.2	492.5	494.2	2.8
	MUE		14.1	3.7	1.4	
	MAX		27.4	6.3	3.1	
Perillaldehyde <i>ax</i> , <i>s</i>	MUE%		1.25	0.37	0.10	
	MAX%		1.60	0.51	0.16	
	A <sup>eq</sup>	1929.7	1957.5	1920.3	1927.2	10.3
	B <sup>eq</sup>	716.4	694.5	715.1	717.2	5.9
	C <sup>eq</sup>	683.6	666.1	682.6	684.6	5.0
	MUE		22.4	3.9	1.4	
	MAX		27.7	9.4	2.5	
	MUE%		2.35	0.27	0.13	
Perillaldehyde <i>eq</i> , <i>s</i>	MAX%		3.05	0.49	0.14	
	A <sup>eq</sup>	2905.5	2877.8	2898.4	2908.1	24.9
	B <sup>eq</sup>	558.7	548.4	555.3	557.2	4.6
	C <sup>eq</sup>	493.1	488.9	492.1	493.8	3.2
	MUE		14.1	3.8	1.6	
	MAX		27.7	7.1	2.6	
	MUE%		1.21	0.35	0.16	
	MAX%		1.84	0.60	0.26	

<sup>a</sup>Absolute mean and maximum unsigned errors between computed and experimental rotational constants (MUE and MAX in MHz) and the corresponding relative values (MUE% and MAX%) are also reported. <sup>b</sup>SE equilibrium rotational constants obtained from the experimental ground state rotational constants given in ref 22 and the HPCS2 vibrational corrections computed in the present work.

12 and 10 lines corresponding to *a*-type transitions were fitted for the {*a*, *a*} and {*g*, *s*} species, respectively. Then, the limited sensitivity of *a*-type transitions to the *A* rotational constant could explain why a strong discrepancy between theory and experiment is observed only for this parameter and only for {*a*, *a*} and {*g*, *s*} thymol.

Within the second family of aliphatic monocyclic species (containing a cyclohexene ring), limonene is classified as a monoterpene, whereas carvone and perillaldehyde are monoterpeneoids, with structures related to isomers of *p*-menthane<sup>3</sup> (see Figure 1). These three molecules are essential oils found in citrus fruit peels, caraway seeds, and perilla herb, respectively. A chiral center is always present, leading to the *R* and *S* enantiomers. However, the absolute configuration will not be considered explicitly, as enantiomers share identical rotational constants.<sup>1</sup>

All low-energy minima of these species (see Table 4) show a half-chair structure of the cyclohexene ring, with atoms 4,5 (limonene and perillaldehyde) or 5,6 (carvone) lying outside the plane occupied by the other four atoms. Then, the hindered rotation around the  $\phi$  dihedral angle (C3–C4–C8 = C9 for limonene, C6–C5–C9 = C10 for carvone, and C3–C4–C9 = C10 for perillaldehyde) generates three low-energy rotamers. Once again, the two rotamers corresponding to  $\phi \approx 120^\circ$  and

$\phi \approx -120^\circ$  will be referred to as *antichiral* (*ac*<sup>+</sup> and *ac*<sup>-</sup>), while the rotamer corresponding to  $\phi \approx 0^\circ$  will be referred to as *synperiplanar* (*s*).

The experimental rotational spectra of limonene,<sup>55</sup> carvone,<sup>55</sup> and perillaldehyde<sup>56</sup> were recorded with a molecular beam Fourier transform microwave (MB-FTMW) spectrometer in the 4–20 GHz region. These studies identified two rotamers for each molecule, both characterized by an equatorial isopropenyl group. More recently, Loru et al.<sup>22</sup> recorded the MW spectra of these three molecules in the 2–8 GHz region. This latter study highlighted greater conformational diversity with respect to earlier findings, identifying four species for limonene, five for carvone, and four for perillaldehyde, including both axial and equatorial conformers.

As shown in Table 5, the BDPCS3 results represent once again a significant improvement over their DPCS3 and, especially, HPCS2 counterparts, approaching the accuracy of 0.1% for all species, except the axial forms of carvone. In this connection, it should be remembered that, contrary to vibrational frequencies, the vibrational corrections of rotational constants computed in the VPT2 framework do not suffer from the presence of resonances,<sup>57</sup> so that accurate and robust results are achieved except in very special cases, characterized by the presence of unusually large cubic force constants involving two

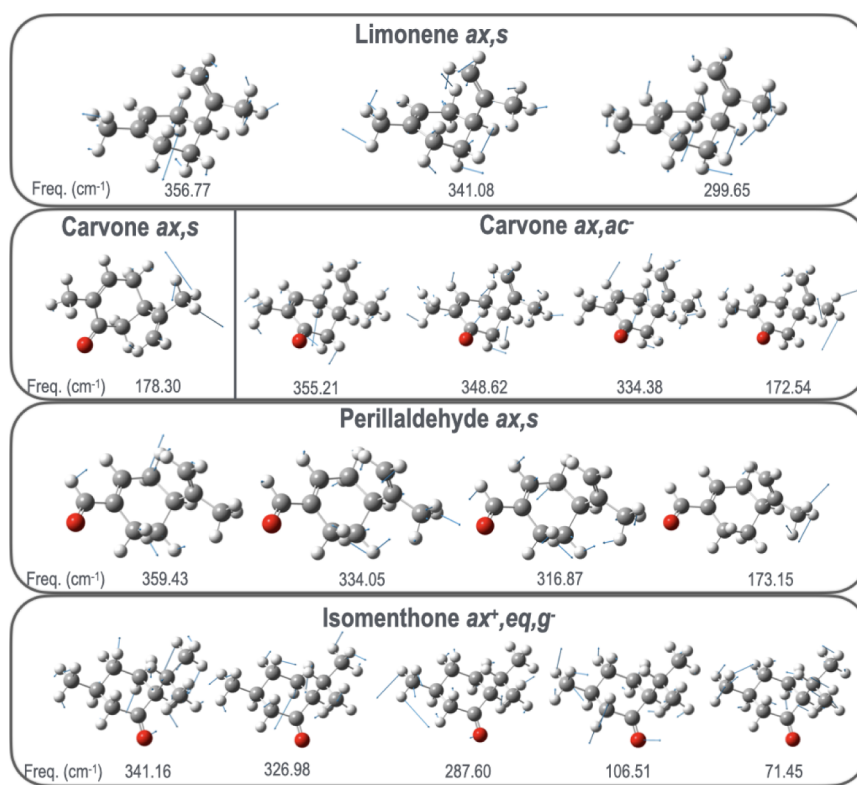


**Figure 3.** Large amplitude motions which are neglected in the evaluation of the anharmonic contribution to vibrational corrections of rotational constants.

different modes. Although a new formulation of VPT2 in curvilinear internal coordinates further reduces the number of problematic situations,<sup>58</sup> this does not help in the present context for a limited number of modes when bulky axial substituents are present in the cyclohexene or (to a lesser extent) cyclohexane rings. For instance, even employing the new VPT2 engine based on internal coordinates, the vibrational corrections for the  $\{ax, s\}$  conformer of limonene are  $-8.5$ ,  $15.9$ , and  $11.3$  MHz, respectively. A reduced-dimensionality model introduced in previous studies<sup>59,60</sup> will be followed, removing the contributions of the problematic normal modes shown in Figure 3. The vibrational corrections obtained in this way for the  $\{ax, s\}$  conformer of limonene ( $20.8$ ,  $6.4$ , and  $5.6$  MHz) are coherent with their counterparts computed by the full VPT2 approach for the other conformers of limonene (see Table 5). The same trend is observed for all other problematic cases (see Tables 5 and 7), but the limitations of the approach could explain the unusually large BDPCS3 errors observed for the axial structures of carvone.

Among the last family of aliphatic monocyclic species (containing a cyclohexane ring), we studied a monoterpene (*p*-menthane) and three monoterpenoids (menthol, menthone, and iso-menthone). While *p*-menthane is an achiral molecule with isopropyl and methyl substituents at C1 and C4, menthol has three chiral centers (C1, C2, and C5), and menthone has two stereogenic centers (C2 and C5). Consequently, diastereoisomeric forms with different rotational constants can be observed for the latter two molecules. We will follow the Cahn–Ingold–Prelog rules<sup>61</sup> to characterize the relative stereochemistry of chiral diastereoisomers.

The low-energy minima of all of these species (see Table 6) are characterized by a chair structure of the cyclohexane ring,

with atoms 1 and 4 lying outside the plane occupied by the other four atoms.

In the case of *p*-menthane, we will consider the structure with both substituents at an equatorial position (refer to the  $\alpha$  values in Table 6). Rotation of the isopropyl group, governed by the dihedral angle  $\phi = H-C7-C1-C2$ , yields two energy minima with  $\phi = -60^\circ$  and  $\phi = 180^\circ$ , corresponding to the  $g^-$  and  $a$  rotamers, respectively. Although both structures could be detectable at least in principle, experimental data are still lacking, possibly because of their low dipole moments.

The MW spectra of (1*R*, 2*S*, 5*R*)-menthol and two menthone diastereoisomers, namely (2*S*, 5*R*)-menthone (commonly referred to as menthone) and (2*R*, 5*R*)-menthone (referred to as isomenthone) were recorded by Schmitzl et al.<sup>23</sup> on a COMPACT spectrometer.

All low-energy minima characterized by our computational workflow for menthol have the three substituents at the equatorial position. The dihedral angle  $\phi = H-C8-C2-C1$  shows energy minima for values around  $60^\circ$  ( $g^+$ ) and  $180^\circ$  ( $a$ ). On the other hand, the energy minima generated by the rotation of the hydroxy group ( $\chi = O-H-C1-C2$ ) fall around  $\pm 60^\circ$  and  $180^\circ$ . The six resulting structures are  $\{\phi, \chi\} = \{g^+, a\}$ ,  $\{g^+, g^-\}$ ,  $\{g^+, g^+\}$ ,  $\{a, a\}$ ,  $\{a, g^-\}$ , and  $\{a, g^+\}$ . However, as already pointed out by Schmitzl et al.,<sup>23</sup> very small energy barriers rule the interconversion between the different rotamers generated by rotation of the  $\chi$  dihedral angle. Therefore, only  $\{g^+, a\}$  and  $\{a, a\}$  species should survive, and the low population estimated for the latter species can explain why only  $\{g^+, a\}$  species has been detected.

Although four low-energy structures might be detected for menthone according to our calculations (see Table 2), the

**Table 6. Relative DPCS3 Electronic Energies ( $\Delta E$ ), HPCS2 Zero-Point Energies ( $\Delta ZPE$ ), Enthalpies [ $\Delta(\Delta H)$ ], and Entropies [ $\Delta(T\Delta S)$ ] at 298.15 K and 1 atm of the Studied Monocyclic Monoterpenes and Monoterpenoids Containing a Cyclohexane ring<sup>a</sup>**

	$\Delta E$	$\Delta ZPE^b$	$\Delta(\Delta H^c)^{cd}$	$\Delta(T\Delta S^e)^{ce}$	$Q^f$	$\theta^f$	$\gamma^f$	$\alpha^g$
<i>p</i> -menthane								
$g^-$	0.0	0.0	0.0	0.0	0.562	1.1	180.0	108.8/71.4
<i>a</i>	2.0	36.0	-26.0	-148.8	0.575	1.4	352.5	103.6/70.9
Menthol								
$g^+, a$	0.0	0.0	0.0	0.0	0.579	1.5	227.8	109.9/76.3/109.2
$g^+, g^-$	79.6	-7.4	16.6	-36.6	0.574	1.5	268.8	106.5/76.0/109.2
$g^+, g^+$	112.4	25.4	-4.5	-75.8	0.579	2.2	239.5	109.8/76.7/109.5
<i>a, a</i>	296.2	12.3	-12.3	-180.2	0.575	1.3	180.0	109.3/74.1/109.0
<i>a, g^-</i>	372.3	18.2	48.7	-59.3	0.571	0.8	205.3	105.5/74.1/109.0
<i>a, g^+</i>	666.8	-35.3	31.1	3.0	0.574	1.5	209.1	109.5/74.5/109.3
Menthone								
<i>eq, eq, g^-</i>	0.0	0.0	0.0	0.0	0.580	1.9	202.1	74.2/109.2
<i>eq, eq, g^+</i>	17.3	-15.2	6.0	55.8	0.556	4.8	346.5	74.2/108.7
<i>eq, eq, a</i>	281.4	-2.2	0.5	-36.4	0.569	2.3	317.4	76.8/137.3
$ax^+, ax^-, g^-$	572.5	94.7	-17.0	40.9	0.560	0.8	201.7	10.6/171.9
Isomenthone								
$ax^+, eq, g^-$	0.0	0.0	0.0	0.0	0.560	2.2	150.1	10.4/71.0
<i>eq, ax^+, g^-</i>	190.8	32.3	-28.2	-142.3	0.580	2.3	182.0	74.2/8.3
<i>eq, ax^+, g^+</i>	209.5	14.2	4.2	-40.1	0.556	3.5	15.0	74.0/7.2
<i>eq, ax^+, a</i>	467.8	36.1	-27.7	-156.5	0.568	0.8	7.5	76.6/7.7

<sup>a</sup>All the energetic values are in  $\text{cm}^{-1}$ , except relative populations. All the geometric parameters are in degrees, except  $Q$ , which is in  $\text{\AA}$ . The atom numbering is shown in Figure 1, and the ordering of rotamers follows their  $\Delta E$ . <sup>b</sup>VPT2 anharmonic value. <sup>c</sup>Harmonic value. <sup>d</sup>Difference between the enthalpy at 298.15 K and 0 K. <sup>e</sup>At 298.15 K. <sup>f</sup>See eqs 1–5 for definitions. All the energy minima correspond to chair structures in which atoms 1 and 4 are outside the plane of the other four atoms. The puckering coordinates of cyclohexane are  $Q = 0.570 \text{ \AA}$ ,  $\theta = 0^\circ$ , and  $\gamma = 0^\circ$  for the chair structure and  $Q = 0.785 \text{ \AA}$ ,  $\theta = 90^\circ$ , and  $\gamma = 0^\circ$  or  $\gamma = 180^\circ$  for the boat structure. <sup>g</sup>These angles indicate the position of the substituent groups in the Cahn–Ingold–Prelog order. For instance, in the menthol case, the first angle corresponds to the position of the hydroxy group, the second one is for the isopropyl group, and the last one is for the methyl group. See the main text for further details.

population of the  $\{ax^+, ax^-, g^-\}$  structure could be too small for its unequivocal detection, when taking into account that the MW spectra were recorded for a mixture of menthone and isomenthone with unknown composition. In fact, only the most stable structure of isomenthone ( $\{ax^+, eq, g^-\}$ ) was detected in the same experiment, possibly due to its low presence in the experimental mixture.

The computed trends of rotational constants (Table 7) align with those of the first two families of monoterpenes and monoterpenoids, with the BDPCS3 model delivering an unprecedented level of accuracy at DFT cost. Overall, the remarkable accuracy of the BDPCS3 rotational constants of menthol, menthone, and isomenthone suggests that the predicted values for *p*-menthane should represent reliable starting points for a future experimental investigation.

As already mentioned, a few outliers were found, with discrepancies in the BDPCS3 rotational constants from their experimental counterparts falling well outside the expected confidence intervals. In this connection, an intuitive picture of the accuracy of the different quantum chemical methods is offered by normal Gaussian distributions defined by

$$\rho(\Delta r) = N_c \exp\left(-\frac{(\Delta r - \Delta r_{\text{av}})^2}{2\Delta r_{\text{Std}}^2}\right) \quad (9)$$

with  $\Delta r_{\text{av}}$  and  $\Delta r_{\text{Std}}$  being the mean signed error and standard deviation, respectively, of the relative percentage error distributions, while  $N_c$  is a suitable normalization constant. Figure 4 provides a graphical representation of the results, while

the numerical data are collected in Table S1. It is remarkable that all systematic errors of the HPCS2 and DPCS3 results (evidenced by non-negligible mean signed errors) are fully corrected at the BDPCS3 level, whose accuracy is further confirmed by a standard deviation close to 0.1%. Furthermore, comparable average signed errors and standard deviations are obtained for the three rotational constants of all the monoterpene classes.

The averaged relative errors of the  $\{a, a\}$  and  $\{g, s\}$  forms of thymol, as well as the  $\{ac, ac\}$  form of estragole, are highlighted by three vertical lines with the same color and style of the associated distribution. It is quite apparent that, for these species, the discrepancies with the experiment of the *A* rotational constants computed by all the employed quantum chemical methods lie well outside the expected confidence intervals, whereas the *B* and *C* constants remain within acceptable ranges. Additional experimental investigation would be required to shed light on this aspect. The other outliers are species with an axial substituent in the cyclohexene ring ( $\{ax, s\}$  and  $\{ax, ac^-\}$  forms of carvone). However, as already mentioned, in those cases, the computed results could have a reduced accuracy due to the necessity of removing some large-amplitude motions from the anharmonic treatment (see Figure 3) related to the extreme sensitivity of puckering coordinates to even small displacements of bulky axial substituents. At the same time, the very low populations computed for these structures cast some doubts on their unequivocal experimental detection.

**Table 7. SE, HPCS2, DPCS3, and BDPCS3 Equilibrium Rotational Constants ( $A^{\text{eq}}$ ,  $B^{\text{eq}}$ , and  $C^{\text{eq}}$  in MHz), together with HPCS2 Vibrational Corrections ( $\Delta\text{Vib}$  in MHz) of the Studied Monocyclic Monoterpenes and Monoterpenoids Containing a Cyclohexane Ring<sup>a</sup>**

	Parameter	SE <sup>b</sup>	HPCS2	DPCS3	BDPCS3	$\Delta\text{Vib}$
<i>p</i> -menthane $g^-$	$A^{\text{eq}}$	—	2801.6	2829.6	2840.3	29.1
	$B^{\text{eq}}$	—	703.7	712.4	715.0	7.6
	$C^{\text{eq}}$	—	593.9	601.4	603.6	6.0
<i>p</i> -menthane <i>a</i>	$A^{\text{eq}}$	—	2759.4	2787.3	2797.6	28.6
	$B^{\text{eq}}$	—	694.0	702.6	705.1	7.9
	$C^{\text{eq}}$	—	640.7	648.8	651.2	6.9
Menthhol $g^+$ , <i>a</i>	$A^{\text{eq}}$	1798.3	1773.9	1791.8	1798.7	18.5
	$B^{\text{eq}}$	700.1	687.9	697.5	699.9	7.5
	$C^{\text{eq}}$	579.1	569.4	576.1	578.1	5.8
	MUE		15.5	4.1	0.5	
	MAX		24.4	6.5	1.0	
	MUE%		1.59	0.42	0.07	
	MAX%		1.75	0.53	0.17	
Menthone <i>eq</i> , <i>eq</i> , $g^-$	$A^{\text{eq}}$	2038.4	2008.5	2030.5	2038.5	16.4
	$B^{\text{eq}}$	700.5	689.1	697.2	699.7	7.0
	$C^{\text{eq}}$	568.0	558.9	565.8	567.9	5.9
	MUE		16.8	4.5	0.3	
	MAX		29.9	7.9	0.8	
	MUE%		1.56	0.41	0.04	
	MAX%		1.63	0.47	0.11	
Menthone <i>eq</i> , <i>eq</i> , $g^+$	$A^{\text{eq}}$	1972.1	1944.4	1965.3	1973.0	18.7
	$B^{\text{eq}}$	701.4	689.3	697.5	699.9	6.8
	$C^{\text{eq}}$	592.9	582.8	590.0	592.1	6.3
	MUE		16.6	4.5	1.0	
	MAX		27.7	6.7	1.4	
	MUE%		1.61	0.46	0.12	
	MAX%		1.72	0.55	0.20	
Menthone <i>eq</i> , <i>eq</i> , <i>a</i>	$A^{\text{eq}}$	2130.7	2100.4	2121.4	2129.1	21.3
	$B^{\text{eq}}$	688.0	676.7	684.9	687.3	6.8
	$C^{\text{eq}}$	604.3	594.3	601.5	603.6	6.2
	MUE		17.2	5.1	1.0	
	MAX		30.3	9.4	1.6	
	MUE%		1.57	0.45	0.10	
	MAX%		1.65	0.46	0.11	
Isomenthone <i>ax</i> <sup>+</sup> , <i>eq</i> , $g^-$	$A^{\text{eq}}$	1545.7	1518.1	1535.0	1541.8	10.4
	$B^{\text{eq}}$	822.1	810.3	820.1	822.6	9.2
	$C^{\text{eq}}$	678.1	670.0	677.7	679.8	6.7
	MUE		16.2	4.8	1.7	
	MAX		27.6	10.7	4.0	
	MUE%		1.52	0.39	0.14	
	MAX%		1.79	0.70	0.26	

<sup>a</sup>Absolute mean and maximum unsigned errors between computed and experimental rotational constants (MUE and MAX in MHz) and the corresponding relative values (MUE% and MAX%) are also provided <sup>b</sup>SE equilibrium rotational constants obtained from the experimental ground state rotational constants given in ref 23 and the HPCS2 vibrational corrections computed in the present work.

#### 4. CONCLUSIONS

The structures and rotational constants of a representative panel of monocyclic monoterpenes and monoterpenoids have been investigated by a new computational strategy approaching the accuracy of state-of-the-art quantum chemical methods at DFT cost. Starting from geometries and harmonic force fields computed by a last-generation double hybrid functional, improved geometrical parameters are obtained by a one-parameter bond correction, and anharmonic contributions to rotational constants by a cheaper hybrid functional in the framework of second-order vibrational perturbation theory. The remarkable agreement of the calculated rotational constants with their experimental counterparts points out the accuracy of

the computed geometries and strongly supports the predicted values for species not yet characterized experimentally. Put in perspective, the accuracy of computed values will enable unbiased interpretation of the spectroscopic parameters of complex molecules in terms of well-defined stereoelectronic effects.

The generality and black-box nature of the computational tool pave the way toward its widespread use for predicting and interpreting high-resolution spectra of molecules containing a few dozen atoms with unprecedented accuracy at a DFT cost. In parallel, the results of the present paper and previous related works<sup>4,5,13,53,54</sup> already provide a comprehensive picture of prototypical molecular bricks of life.

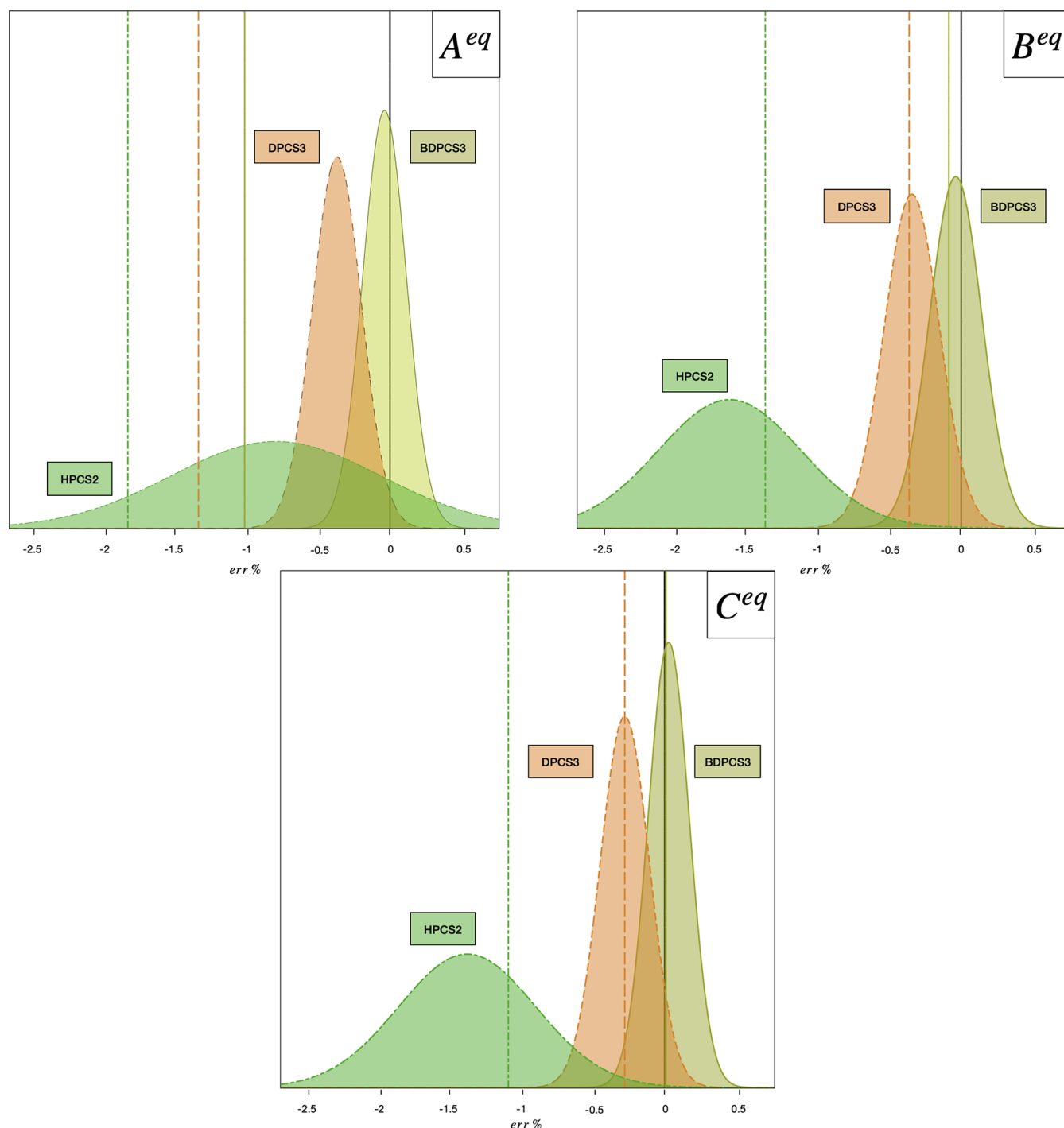


**Figure 4.** Gaussian normal distributions of the relative percentage errors of  $A^{eq}$ ,  $B^{eq}$ , and  $C^{eq}$  rotational constants computed by different methods with respect to their SE counterparts. The average and standard deviation are computed for the whole set of species for which experimental data are available. The vertical lines represent the averages of the relative percentage errors (along the axis considered) for the three outliers containing a benzene ring: thymol { $a$ ,  $a$ }, thymol { $g$ ,  $s$ }, and estragole { $ac$ ,  $ac$ }. The employed quantum chemical models are identified by different colors.

## ■ ASSOCIATED CONTENT

### SI Supporting Information

The Supporting Information is available free of charge at <https://pubs.acs.org/doi/10.1021/acs.jpca.4c07181>.

Statistical error analysis of computed rotational constants (Tables S1 and S2) and DPCS3 equilibrium geometries (PDF)

## ■ AUTHOR INFORMATION

### Corresponding Author

Vincenzo Barone – *INSTM, Firenze 50121, Italy*;  
orcid.org/0000-0001-6420-4107;  
Email: vincebarone52@gmail.com

### Authors

Federico Lazzari – *Scuola Normale Superiore di Pisa, Pisa 56126, Italy*; orcid.org/0000-0003-4506-3200

Lina Uribe — *Scuola Normale Superiore di Pisa, Pisa 56126, Italy; Scuola Superiore Meridionale, Napoli 80138, Italy*  
Silvia Di Grande — *Scuola Normale Superiore di Pisa, Pisa 56126, Italy; Scuola Superiore Meridionale, Napoli 80138, Italy*; [orcid.org/0000-0002-6550-0220](https://orcid.org/0000-0002-6550-0220)  
Luigi Crisci — *Scuola Normale Superiore di Pisa, Pisa 56126, Italy*; [orcid.org/0000-0002-8140-5397](https://orcid.org/0000-0002-8140-5397)  
Marco Mendolicchio — *Scuola Normale Superiore di Pisa, Pisa 56126, Italy*; [orcid.org/0000-0002-4504-853X](https://orcid.org/0000-0002-4504-853X)

Complete contact information is available at:  
<https://pubs.acs.org/10.1021/acs.jpca.4c07181>

## Notes

The authors declare no competing financial interest.

## ACKNOWLEDGMENTS

Funding from Gaussian Inc. is gratefully acknowledged.

## REFERENCES

- (1) Clayden, J.; Greeves, N.; Warren, S. *Organic Chemistry*; OUP Oxford, 2012.
- (2) Perveen, S.; Al-Taweel, A. M.; Blumenberg, M. *Terpenes and Terpenoids: recent Advances*; International series of monographs on physics; BoD—Books on Demand, 2021.
- (3) Breitmaier, E. *Terpenes: flavors, Fragrances, Pharmaca, Pheromones*; John Wiley & Sons, 2006.
- (4) Uribe, L.; Lazzari, F.; Di Grande, S.; Crisci, L.; Mendolicchio, M.; Barone, V. Accurate Structures and Rotational Constants of Bicyclic Monoterpenes at DFT Cost by Neans of the Bond-Corrected Pisa Composite Scheme (BPCS). *J. Chem. Phys.* **2024**, *161* (1), 014307.
- (5) Barone, V. Quantum Chemistry Meets High-Resolution Spectroscopy for Characterizing the Molecular Bricks of Life in the Gas-Phase. *Phys. Chem. Chem. Phys.* **2024**, *26*, 5802–5821.
- (6) Di Grande, S.; Barone, V. Toward Accurate Quantum Chemical Methods for Molecules of Increasing Dimension: The New Family of Pisa Composite Schemes. *J. Phys. Chem. A* **2024**, *128*, 4886–4900.
- (7) Di Grande, S.; Lazzari, F.; Barone, V. Accurate Geometries of Large Molecules at DFT Cost by Semiexperimental and Coupled Cluster Templating Fragments. *J. Chem. Theory Comput.* **2024**, *20*, 9243–9258.
- (8) Adler, T. B.; Knizia, G.; Werner, H.-J. A Simple and Efficient CCSD(T)-F12 Approximation. *J. Chem. Phys.* **2007**, *127* (22), 221106.
- (9) Knizia, G.; Adler, T. B.; Werner, H.-J. Simplified CCSD(T)-F12 methods: Theory and benchmarks. *J. Chem. Phys.* **2009**, *130* (5), 054104.
- (10) Barone, V. Accuracy Meets Feasibility for the Structures and Rotational Constants of the Molecular Bricks of Life: A Joint Venture of DFT and Wave-Function Methods. *J. Phys. Chem. Lett.* **2023**, *14*, 5883–5890.
- (11) Puzzarini, C.; Stanton, J. F. Connections between the Accuracy of Rotational Constants and Equilibrium Molecular Structures. *Phys. Chem. Chem. Phys.* **2023**, *25*, 1421–1429.
- (12) Barone, V. PCS/Bonds and PCS0: Pick Your Molecule and Get Its Accurate Structure and Ground State Rotational Constants at DFT Cost. *J. Chem. Phys.* **2023**, *159* (8), 081102.
- (13) Barone, V.; Lazzari, F. Hunting for Complex Organic Molecules in the Interstellar Medium: The Role of Accurate Low-Cost Theoretical Geometries and Rotational Constants. *J. Phys. Chem. A* **2023**, *127*, 10517–10527.
- (14) Nielsen, H. H. The Vibration-Rotation Energies of Molecules. *Rev. Mod. Phys.* **1951**, *23*, 90–136.
- (15) Mills, I. M. *Molecular Spectroscopy: Modern Research*; Rao, K N; Matthews, C W eds.; Elsevier, 2012.
- (16) Barone, V. Anharmonic Vibrational Properties by a Fully Automated Second Order Perturbative Approach. *J. Chem. Phys.* **2005**, *122* (1), 014108.
- (17) Mendolicchio, M.; Bloino, J.; Barone, V. General Perturb-Then-Diagonalize Model for the Vibrational Frequencies and Intensities of Molecules Belonging to Abelian and Non-Abelian Symmetry Groups. *J. Chem. Theory Comput.* **2021**, *17*, 4332–4358.
- (18) Franke, P. R.; Stanton, J. F.; Douberly, G. E. How to VPT2: Accurate and Intuitive Simulations of CH Stretching Infrared Spectra Using VPT2+K with Large Effective Hamiltonian Resonance Treatments. *J. Phys. Chem. A* **2021**, *125*, 1301–1324.
- (19) Calabrese, C.; Gou, Q.; Maris, A.; Melandri, S.; Caminati, W. Conformational Equilibrium and Internal Dynamics of E-Anethole: A Rotational Study. *J. Phys. Chem. B* **2016**, *120*, 6587–6591.
- (20) Godfrey, P. D.; McNaughton, D.; Evans, C. J. The Millimetre-Wave Spectrum of Estragole. *Chem. Phys. Lett.* **2013**, *580*, 37–42.
- (21) Schmitz, D.; Shubert, V. A.; Giuliano, B. M.; Schnell, M. The Broadband Microwave Spectra of the Monoterpenoids Thymol and Carvacrol: Conformational Landscape and Internal Dynamics. *J. Chem. Phys.* **2014**, *141*, 034304.
- (22) Loru, D.; Vigorito, A.; Santos, A. F.; Tang, J.; Sanz, M. E. The Axial/Equatorial Conformational Landscape and Intramolecular Dispersion: New Insights from the Rotational Spectra of Monoterpenoids. *Phys. Chem. Chem. Phys.* **2019**, *21*, 26111–26116.
- (23) Schmitz, D.; Schubert, V. A.; Betzl, T.; Schnell, M. Exploring the Conformational Landscape of Menthol, Menthone, and Isomenthone: A Microwave Study. *Frontiers Chem.* **2015**, *3*, 15.
- (24) Bannwarth, C.; Ehlert, S.; Grimme, S. GFN2-xTB, an Accurate and Broadly Parametrized Self-Consistent Tight-Binding Quantum Chemical Method With Multipole Electrostatics and Density-Dependent Dispersion Contributions. *J. Chem. Theory Comput.* **2019**, *15*, 1652–1671.
- (25) Pracht, P.; Bohle, F.; Grimme, S. Automated Exploration of the Low-Energy Chemical Space With Fast Quantum Chemical Methods. *Phys. Chem. Chem. Phys.* **2020**, *22*, 7169–7192.
- (26) Becke, A. D. Density-Functional Exchange-Energy Approximation with Correct Asymptotic Behavior. *Phys. Rev. A* **1988**, *38*, 3098–3100.
- (27) Lee, C.; Yang, W.; Parr, R. G. Development of the Colle-Salvetti Correlation-Energy Formula Into a Functional of the Electron Density. *Phys. Rev. B* **1988**, *37*, 785–789.
- (28) Becke, A. D. Density-functional thermochemistry. III. The role of exact exchange. *J. Chem. Phys.* **1993**, *98* (7), 5648–5652.
- (29) Hrehre, W. J.; Ditchfield, R.; Pople, J. A. Self-Consistent Molecular Orbital Methods. XII. Further Extensions of Gaussian-Type Basis Sets for Use in Molecular Orbital Studies of Organic Molecules. *J. Chem. Phys.* **1972**, *56*, 2257–2261.
- (30) Hariharan, P. C.; Pople, J. A. The Influence of Polarization Functions on Molecular Orbital Hydrogenation Energies. *Theor. Chim. Acta.* **1973**, *28*, 213–222.
- (31) Clark, T.; Chandrasekhar, J.; Spitznagel, G. W.; Schleyer, P. V. R. Efficient Diffuse Function-Augmented Basis Sets for Anion Calculations. III. The 3-21+G Basis Set for First-Row Elements, Li-F. *J. Comput. Chem.* **1983**, *4*, 294–301.
- (32) Grimme, S.; Antony, J.; Ehrlich, S.; Krieg, H. A Consistent and Accurate *Ab Initio* Parametrization of Density Functional Dispersion Correction (DFT-D) for the 94 Elements H-Pu. *J. Chem. Phys.* **2010**, *132* (15), 154104.
- (33) Grimme, S.; Ehrlich, S.; Goerigk, L. Effect of the Damping Function in Dispersion Corrected Density Functional Theory. *J. Comput. Chem.* **2011**, *32*, 1456–1465.
- (34) Santra, G.; Sylvetsky, N.; Martin, J. M. Minimally Empirical Double-Hybrid Functionals Trained Against the GMTKN55 Database: RevDSD-PBEP86-D4, revDOD-PBE-D4, and DOD-SCAN-D4. *J. Phys. Chem. A* **2019**, *123*, 5129–5143.
- (35) Peterson, K. A.; Adler, T. B.; Werner, H.-J. Systematically convergent basis sets for explicitly correlated wavefunctions: The atoms H, He, B–Ne, and Al–Ar. *J. Chem. Phys.* **2008**, *128* (8), 084102.
- (36) Dunning, T. H. Gaussian Basis Sets for Use in Correlated Molecular Calculations. I. The Atoms Boron Through Neon and Hydrogen. *J. Chem. Phys.* **1989**, *90*, 1007–1023.

- (37) Alonso, E. R.; León, I.; Alonso, J. L. *Intra- and Intermolecular Interactions Between Non-Covalently Bonded Species*; Elsevier, 2020; pp. 93–141.
- (38) León, I.; Fusè, M.; Alonso, E. R.; Mata, S.; Mancini, G.; Puzzarini, C.; Alonso, E. R.; Barone, V. Unbiased Disentanglement of Conformational Baths With the Help of Microwave Spectroscopy, Quantum Chemistry and Artificial Intelligence: The Puzzling Case of Homocysteine. *J. Chem. Phys.* **2022**, *157* (7), 074107.
- (39) Ruoff, R. S.; Klots, T. D.; Emilsson, T.; Gutowsky, H. S. Relaxation of Conformers and Isomers in Seeded Supersonic Jets of Inert Gases. *J. Chem. Phys.* **1990**, *93*, 3142–3150.
- (40) Godfrey, P. D.; Brown, R. D. Proportions of Species Observed in Jet Spectroscopy-Vibrational Energy Effects: Histamine Tautomers and Conformers. *J. Am. Chem. Soc.* **1998**, *120*, 10724–10732.
- (41) Florio, G. M.; Christie, R. A.; Jordan, K. D.; Zwier, T. S. Conformational Preferences of Jet-Cooled Melatonin: Probing Trans- and Cis-Amide Regions of the Potential Energy Surface. *J. Am. Chem. Soc.* **2002**, *124*, 10236–10247.
- (42) Cremer, D. T.; Pople, J. A. General Definition of Ring Puckering Coordinates. *J. Am. Chem. Soc.* **1975**, *97*, 1354–1358.
- (43) Cremer, D. A General Definition of Ring Substituent Positions. *Isr. J. Chem.* **1980**, *20*, 12–19.
- (44) Chan, L.; Hutchison, G. R.; Morris, G. M. Understanding Ring Puckering in Small Molecules and Cyclic Peptides. *J. Chem. Inf. Model* **2021**, *61*, 743–755.
- (45) Demaison, J. Experimental, Semi-Experimental and Ab Initio Equilibrium Structures. *Mol. Phys.* **2007**, *105*, 3109–3138.
- (46) Watrous, A. G.; Westbrook, B. R.; Fortenberry, R. C. F12-TZ-cCR: A methodology for faster and still highly-accurate quartic force fields. *J. Phys. Chem. A* **2021**, *125*, 10532–10540.
- (47) Mendolicchio, M.; Penocchio, E.; Licari, D.; Tassinato, N.; Barone, V. Development and Implementation of Advanced Fitting Methods for the Calculation of Accurate Molecular Structures. *J. Chem. Theory Comput.* **2017**, *13*, 3060–3075.
- (48) Piccardo, M.; Penocchio, E.; Puzzarini, C.; Biczysko, M.; Barone, V. Semi-Experimental Equilibrium Structure Determinations by Employing B3LYP/SNSD Anharmonic Force Fields: Validation and Application to Semirigid Organic Molecules. *J. Phys. Chem. A* **2015**, *119*, 2058–2082.
- (49) Lazzari, F.; Mendolicchio, M.; Barone, V. Accurate Geometries of Large Molecules by Integration of the Pisa Composite Scheme and the Templating Synthron Approach. *J. Phys. Chem. A* **2024**, *128*, 1385–1395.
- (50) Cordero, B.; Gomez, V.; Platero-Prats, A. E.; Revés, M.; Echevarria, J.; Cremades, E.; Barragan, F.; Alvarez, S. Covalent Radii Revisited. *Dalton Trans.* **2008**, No. 21, 2832–2838.
- (51) Pauling, L. Atomic Radii and Interatomic Distances in Metals. *J. Am. Chem. Soc.* **1947**, *69*, 542–553.
- (52) Frisch, M. J.; Trucks, G. W.; Schlegel, H. B.; Scuseria, G. E.; Robb, M. A.; Cheeseman, J. R.; Scalmani, G.; Barone, V.; Petersson, G. A.; Nakatsuji, H., et al. *Gaussian 16 Revision C.01*; Gaussian Inc: Wallingford CT, 2016.
- (53) Barone, V.; Fusè, M.; Lazzari, F.; Mancini, G. Benchmark Structures and Conformational Landscapes of Amino Acids in the Gas Phase: A Joint Venture of Machine Learning, Quantum Chemistry, and Rotational Spectroscopy. *J. Chem. Theory Comput.* **2023**, *19*, 1243–1260.
- (54) Uribe, L.; Di Grande, S.; Crisci, L.; Lazzari, F.; Mendolicchio, M.; Barone, V. Accurate Structures and Rotational Constants of Steroid Hormones at DFT Cost: Androsterone, Testosterone, Estrone,  $\beta$ -Estradiol, and Estriol. *J. Phys. Chem. A* **2024**, *128*, 2629–2642.
- (55) Moreno, J. R. A.; Huet, T. R.; González, J. J. L. Conformational Relaxation of S-(+)-Carvone and R-(+)-Limonene Studied by Microwave Fourier Transform Spectroscopy and Quantum Chemical Calculations. *Struct. Chem.* **2013**, *24*, 1163–1170.
- (56) Moreno, J. R. A.; Ureña, F. P.; González, J. J. L.; Huet, T. R. Terpenes in the Gas Phase: The Structural Conformation of S-(–)-Perillaldehyde Investigated by Microwave Spectroscopy and Quantum Chemical Calculations. *Chem. Phys. Lett.* **2009**, *473*, 17–20.
- (57) Mendolicchio, M.; Barone, V. Unbiased Comparison Between Theoretical and Experimental Molecular Structures and Properties: Toward an Accurate Reduced-Cost Evaluation of Vibrational Corrections. *J. Chem. Theory Comput.* **2024**, *20*, 2842–2857.
- (58) Mendolicchio, M.; Barone, V. Accurate Vibrational and Rotational Contributions to the Properties of Large Molecules by a New Engine Employing Curvilinear Internal Coordinates and Vibrational Perturbation Theory to Second Order. *J. Chem. Theory Comput.* **2024**, *20*, 8378–8395.
- (59) Ceselin, G.; Salta, Z.; Bloino, J.; Tassinato, N.; Barone, V. Accurate Quantum Chemical Spectroscopic Characterization of Glycolic Acid: A Route Toward its Astrophysical Detection. *J. Phys. Chem. A* **2022**, *126*, 2373–2387.
- (60) Alessandrini, S.; Ye, H.; Biczysko, M.; Puzzarini, C. Describing the Disulfide Bond: From the Density Functional Theory and Back Through the “Lego Brick” Approach. *J. Phys. Chem. A* **2024**, *128*, 9383–9397.
- (61) Cahn, R. S.; Ingold, C.; Prelog, V. Specification of Molecular Chirality. *Angew. Chem., Int. Ed.* **1966**, *5*, 385–415.